Reluctance network model of open-loop Hall-effect current sensor for circuit-type simulation software analyses

Atef Lekdim, Fabien Sixdenier, Riccardo Scorretti, Adnan Grihe

AUTHOR QUERIES

AUTHOR PLEASE ANSWER ALL QUERIES

PLEASE NOTE: We cannot accept new source files as corrections for your article. If possible, please annotate the PDF proof we have sent you with your corrections and upload it via the Author Gateway. Alternatively, you may send us your corrections in list format. You may also upload revised graphics via the Author Gateway.

Carefully check the page proofs (and coordinate with all authors); additional changes or updates WILL NOT be accepted after the article is published online/print in its final form. Please check author names and affiliations, funding, as well as the overall article for any errors prior to sending in your author proof corrections. Your article has been peer reviewed, accepted as final, and sent in to IEEE. No text changes have been made to the main part of the article as dictated by the editorial level of service for your publication.

AQ:1 = According to our records, Fabien Sixdenier is listed as a Member, IEEE. Please verify.

AQ:2 = Please confirm or add details for any funding or financial support for the research of this article.

AQ:3 = Please provide the expansion of the acronym LEM for your funding agency. Providing the correct acknowledgment will ensure proper credit to the funder.

AQ:4 = Please confirm whether the edits made in the current affiliations of the authors Fabien Sixdenier and Riccardo Scorretti are correct.

AQ:5 = Please provide the department names for the University of Lyon and Université Claude Bernard Lyon 1.

AQ:6 = Please provide the full current affiliation details (department name, name of university/institution, city, state/country, zip/postal code) for the author Adnan Grihe.

AQ:7 = Please provide updated assembled images for Figs. 19 by updating quality if needed.

AQ:8 = Please provide the publisher name and publisher location for Ref. [7].

AQ:9 = Please provide the publisher location for Ref. [8].

AQ:10 = Author photos appear to be too blurry. Please provide a better quality/higher resolution photos for the authors Fabien Sixdenier, Riccardo Scorretti, and Adnan Grihe.

Reluctance Network Model of Open-Loop Hall-Effect Current Sensor for Circuit-Type Simulation Software Analyses

AQ:1 Atef Lekdim, Fabien Sixdenier, *Member, IEEE*, Riccardo Scorretti, and Adnan Grihe

***Abstract*—The automotive industry progresses towards full electrification of cars. Therefore, more and more current sensors will be used in each car. These sensors must consume little electrical energy and be as cheap as possible due to the cost-sensitive automotive market. The latter leads to the use, where possible, of Hall-effect open-loop sensors composed of cheap magnetic materials, such as Fe-Si alloys for the magnetic circuit. Depending on the wide range of current and bandwidth of the different onboard electrical devices, each sensor has a different magnetic circuit that must be designed quickly but still accurately. This paper aims to facilitate the design work of engineers by providing them with a simulation model that can be easily used in a circuit type simulation software such as LTspice. This model can bring high-fidelity results in terms of sensor linearity and frequency bandwidth which allows the optimization of the sensor before proceeding to the prototyping step, reducing the time and costs of the design phase.**

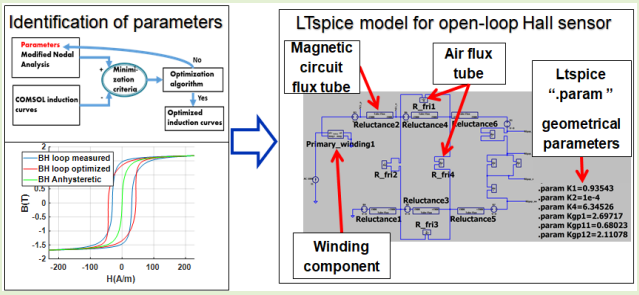

***Index Terms*—SPICE, finite element analysis, magnetic flux density, current measurement.**

I. Introduction

SIMULATIONS are of high importance for design purposes to improve electrical devices. In current sensors, especially Hall effect sensors, Finite Element (FE) simulations are of great help to optimize the magnetic circuit size and shape. All sensor dimensions must be optimized depending on the maximum current to be measured, the electromagnetic environment, and the bus-bar size. The air-gap length is one of the most important parameters to set correctly because it defines, among other things, the linearity limit of the sensor. However, especially simulating several current levels to obtain linearity curves is time-consuming and requires high computing power.

AQ:2 AQ:3 Manuscript received February 24, 2022; accepted April 16, 2022. This work was supported by the collaboration between LEM Tech France and the Ampère Laboratory of the Claude Bernard Lyon 1 University. The associate editor coordinating the review of this article and approving it for publication was Prof. Boby George. *(Corresponding author: Atef Lekdim.)*

Atef Lekdim is with LEM Tech France SAS, 69800 Saint-Priest, France (e-mail: ale@lem.com).

AQ:4 AQ:5 Fabien Sixdenier and Riccardo Scorretti are with the University of Lyon, 69361 Lyon, France, also with Université Claude Bernard Lyon 1, 69100 Villeurbanne, France, also with the INSA Lyon, 69621 Villeurbann, France, and also with the Ampère Laboratory, CNRS, UMR5005, École Centrale de Lyon, 69622 Villeurbanne, France (e-mail: fabien.sixdenier@univ-lyon1.fr; riccardo.scorretti@ec-lyon.fr).

AQ:6 Adnan Grihe was with LEM Tech France SAS, 69800 Saint-Priest, France. He is now with ??? (e-mail: adnan.grihe@gmail.com).

Digital Object Identifier 10.1109/JSEN.2022.3169920

Moreover, to obtain the frequency bandwidth, several FE time-domain simulations must be done (one per frequency). All these simulations can take several days or even weeks to complete.

One faster alternative is to take advantage of the electrical and magnetic analogy, and to model the magnetic circuit based on an equivalent magnetic network. The equivalent magnetic network modelling is widely used in electrical machines [1]–[4]. The equivalent magnetic network is also used in less complicated systems as shown in [5] and [6]. The authors in [5] have studied an oblong magnetic circuit without airgap excited by one winding. The equivalent magnetic network is composed of 28 magnetic reluctances which is enough to model local dynamic phenomena. Previously, the authors in [6] have studied a circular magnetic circuit with airgap for a closed-loop Hall effect sensor. Their equivalent magnetic circuit is composed of only 5 magnetic reluctances, because dynamic effects are considered differently (averaging homogenization) than in [5]. In this paper, the method developed in [6] is adapted in a more generalized way and applied to two oblong geometries. The goal of this part of the work is to develop a generic magnetic reluctance network topology to guarantee the reproducibility of the method for a large spectrum of magnetic circuit geometry/dimensions.

The main advantage of this approach is that the equivalent magnetic circuit can be easily implemented in an electrical

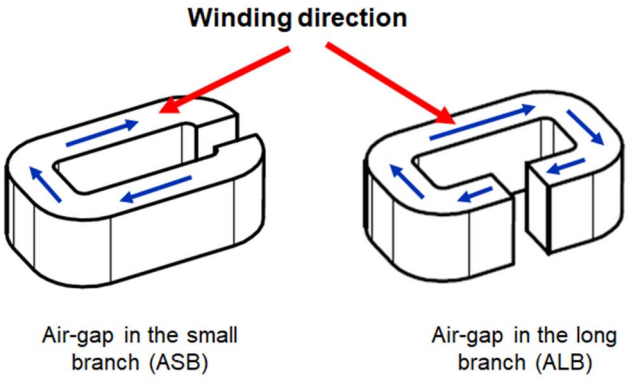

Fig. 1. Oblong wound magnetic cores fabricated with Fe-Si tape of 0.23 mm thickness.

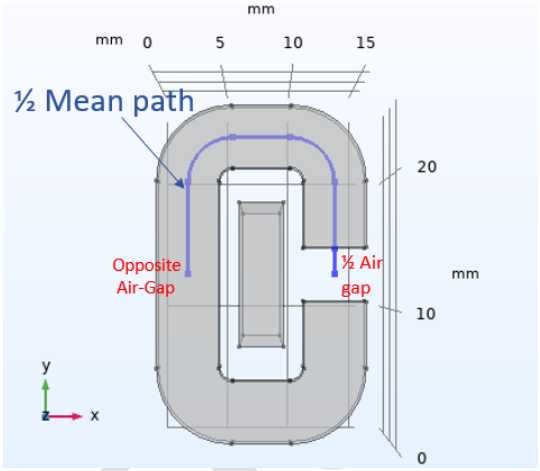

Fig. 2. 3D COMSOL model of ALB magnetic core and the tracing path of the magnetic flux density in the xy plane.

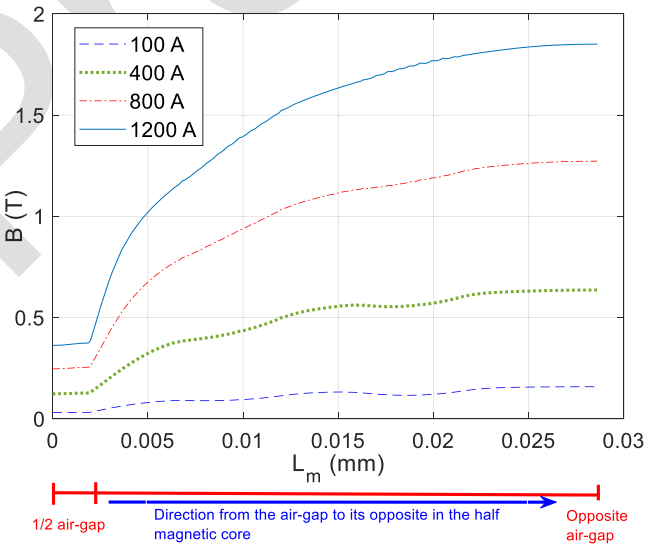

Fig. 3. Magnetic flux density distribution over the half of the mean length L_m of the ALB geometry for four simulated DC currents.

circuit software such as LTspice. Furthermore, one can couple it to an electronic circuit and simulate the whole sensor in a fast way. Once identified, the model can give several useful pieces of information (sensor gain, time response, linearity, frequency bandwidth…) in a very short time.

The next section describes the modelling methodology that we used to model the magnetic circuit with sufficient accuracy. The third section will present some results given by our model compared to experimental measurements. Before the conclusion part, a table is given to compare the proposed model to others published in literature.

II. Modelling Methodology

Our modelling methodology is separated into two main parts. First, the geometric parameters of a magnetic equivalent network are identified at different DC current levels. Second, with the same network topology and the best identified geometric parameters, dynamic flux circuit tubes and specific components able to work in transient simulations are created. The components are put in place in the model to determine the sensor linearity, frequency bandwidth and response time.

A. Magnetic Core Geometries

To show that the method is generic, it is applied on two oblong magnetic cores with the same mechanical dimensions, but with different air gap localizations. Fig. 1 presents the studied magnetic cores. They are fabricated with silicon steel tape, wound on an oblong mandrel. The figure at the left exhibits the airgap in the small branch (ASB) and at right the air-gap in the long branch (ALB).

B. First Finite Element Stationary Simulation on COMSOL

The goal of these preliminary FE stationary simulations is to have an idea about the magnetic flux density distribution along the magnetic circuit and in the external environment (fringing flux) to propose a representative reluctance network model. The simulations have been done with COMSOL in 3D mode for different primary DC current levels. Indeed, it is important to validate the reluctance model for complete current measuring range (up to 1200 A). Thus, parametric simulation was done to obtain the magnetic flux density distribution along the mean length of the magnetic circuit and along the air gap. This flux density distribution will be used as a reference by the optimization algorithm. For the rest of this section, we present only the simulation results of the ALB geometry. The conclusions for the ASB geometry are very similar.

Fig. 2 shows the ALB model and the mean path used to plot the magnetic flux density. The geometric and physical symmetries allow modelling of only the half of the magnetic circuit.

Fig. 3 exhibits the stationary simulation results in term of magnetic flux density distribution along the half mean path as presented in Fig. 2. The simulation was done for 12 current levels (100 to 1200 A).

Fig. 3 shows that for all values of current (only 4 out of 12 represented), the induction starts from its minimum in the air gap to its maximum at the opposite side of the air-gap.

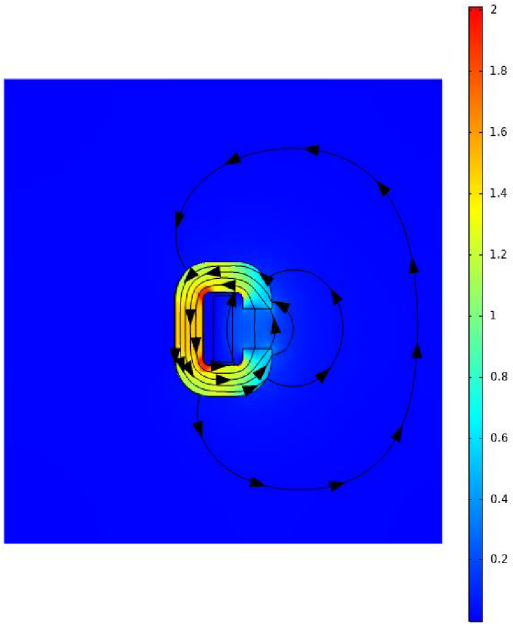

Fig. 4. Flux density (color scale) and flux lines of the ALB geometry are presented in the xy plane. The simulation was done at 400 A primary current.

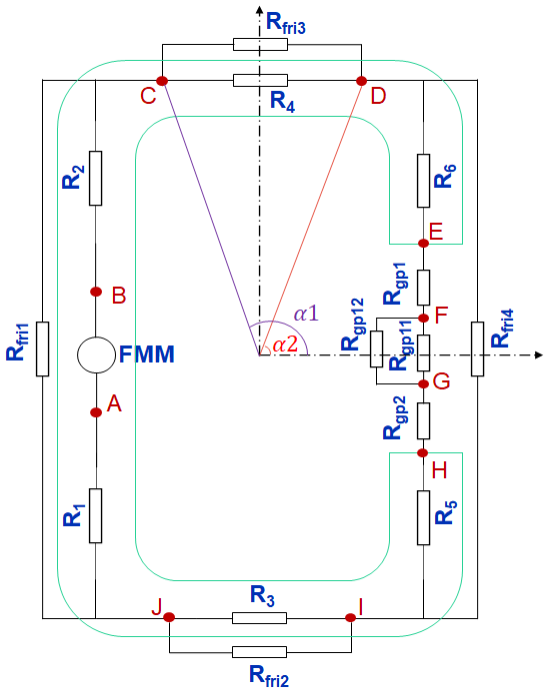

Fig. 5. Generic reluctance network topology applied to the ALB geometry. This topology will reproduce the flux density distribution inside the core and in the air-gape and the distribution of the fringing field in the air area around the magnetic core.

The flux density increases non-linearly with the mean length. We can also notice that for $I_P = 1200$ A the induction reaches the practical saturation level of the Fe-Si material (1.85 T). This indicates that the measuring limit is close to 1200 A in this case. For the other curves, the maximum induction does not reach practical saturation levels. These curves will be used later for the identification of the geometric parameters.

C. Reluctance Network Topology

To propose a representative topology, we used the COMSOL stationary simulation to visualize the fringing flux lines. Fig. 4 shows the flux density on a color scale, and flux lines in the xy plane.

The figure shows clearly that the flux density distribution is non-homogenous inside the core, and it decreases from the opposite side of the air-gap to the air-gap. Indeed, the flux density decreasing is the result of the fringing field diverting from the magnetic material. Thus, the evolution of these two magnetic properties is antagonistic. The fringing flux lines are mainly located in the interior core volume (the hole of the sensor) and in the exterior core volume near the air-gap.

To consider the fringing flux, we propose the reluctance network of Fig. 5.

The reluctances R_1 to R_6 represent the magnetic circuit split into several parts. The reluctance R_{fri1} determines the fringing flux inside the hole of the core and R_{fri2} to R_{fri4} reproduce the fringing flux distribution outside the magnetic core volume. In the ALB and ASB geometries, the R_{fri2} and R_{fri3} should not be necessary because the COMSOL simulation did not show any fringing flux lines in these regions. We still leave them in place in the identification process. If they have a negligible effect, the optimization algorithm should return parameters leading to negligible flux in these reluctances.

The reluctances R_{gp1}, R_{gp2}, R_{gp11} and R_{gp12} reproduce the air-gap magnetic behaviour. The length of each reluctance is calculated according to the dimensions of the magnetic circuit and the fictitious angles α_1 and α_2.

D. Parameter Identification

An optimization method is used for the identification of the parameters.

1) Geometric Parameter Identification: The following geometric parameters are all defined relatively as ratios of cross sections.

$$K_1 = \frac{S_{fri1}}{S_{cm}};\quad K_2 = K_3 = \frac{S_{fri2}}{S_{cm}};\quad K_4 = \frac{S_{fri4}}{S_{cm}}$$

$$K_{gp1} = K_{gp2} = \frac{S_{gp1}}{S_{cm}};\quad K_{gp11} = \frac{S_{gp11}}{S_{cm}};\quad K_{gp12} = \frac{S_{gp12}}{S_{cm}}.$$

S_{cm} is the magnetic circuit cross-section. S_{fri1} to S_{fri4} define the fringing flux cross-sections of reluctances R_{fri1} to R_{fri4} respectively.

S_{gp1}, S_{gp2}, S_{gp11}, S_{gp12} define the surfaces of reluctances R_{gp1}, R_{gp2}, R_{gp11}, R_{gp12} that represent the fringing fluxes in the air- gap.

For each DC current level, the simulated curve of the induction distribution in the magnetic circuit from COMSOL is compared to the one given by the reluctance network model. The objective function (minimization criteria) is the quadratic error between these two curves (see [6] for details). The reluctance network is modelled using the "Modified Nodal Analysis" which is used in SPICE type software [7], [8].

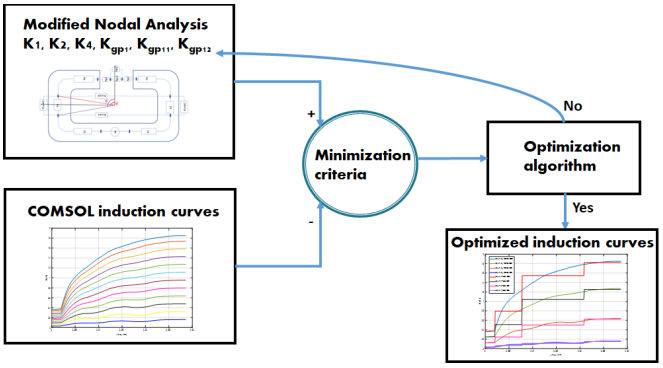

Fig. 6. Geometric parameter optimization diagram. The geometric parameters are modified according to the COMSOL curves until the tolerance is respected in the minimization criteria.

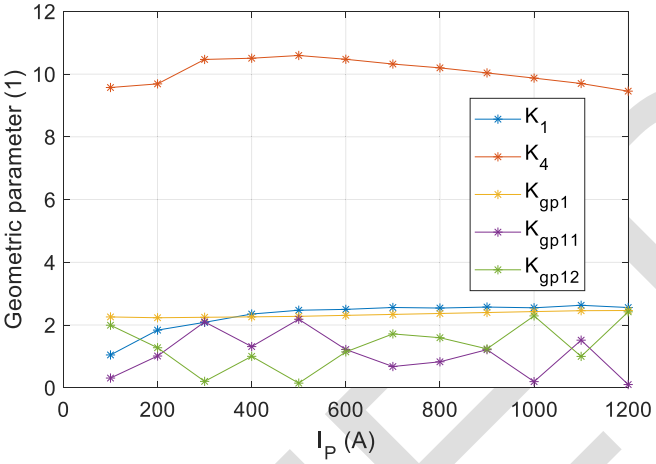

Fig. 7. Variation of the geometric parameters as a function of the applied primary current I_p for the ALB magnetic circuit.

Concretely, the optimization loop of Fig. 6 changes the geometric parameters (the ratios K_1, K_2, K_3, K_4, K_{gp1}, K_{gp11} and K_{gp12}) so that the difference between flux density obtained by COMSOL simulation "B_{COMSOL}" and that one calculated from the model "B_{MODEL}" is minimized.

First, the optimization algorithm found that K_2 and K_3 had a very low value. Doing so, the algorithm confirms that reluctances R_{fri2} and R_{fri3} are not necessary for this magnetic circuit shape. Therefore, the corresponding values K_2, K_3 are removed in Fig. 7.

Secondly, we notice that the values of K_1, K_4, K_{gp1}, are not very sensitive to the level of current. K_1 and K_{gp1} values are approximately equal to 2. This means that there is some fringing flux in the hole of the ALB core and in the air-gap. However, K_4 represents the whole fringing flux outside the core and is evaluated at approximately 10. This means that there is a massive 3D fringing flux due to the large air-gap. K_{gp11}, K_{gp12} slightly depend on the current level, but their changes cancel each other. For all these reasons, it is possible to define only one set of geometric parameters that will be valid for all current values. Table I summarizes the set of parameters that was adopted (mean value of each parameter for all current values).

TABLE I
SET OF THE GEOMETRIC PARAMETERS

	Mean value
K_1	2.31
K_4	10.07
K_{gp1}, K_{gp2}	2.34
K_{gp11}	1.05
K_{gp12}	1.33

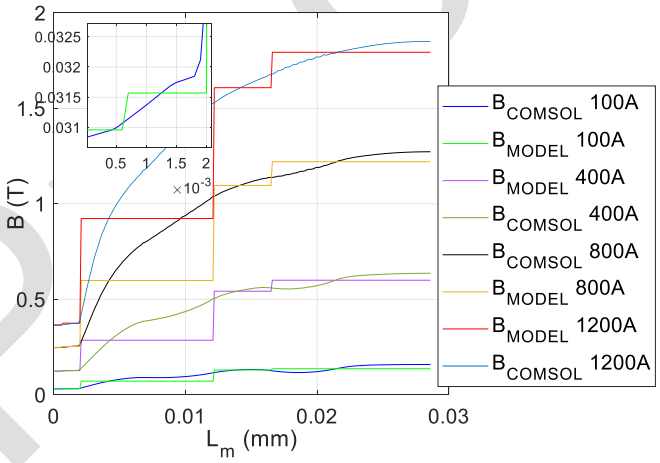

Fig. 8. Comparison between B_{MODEL} and B_{COMSOL} distribution for several primary currents Ip using a unique set of geometric parameters of the ALB magnetic circuit.

The use of the parameters of table I ends up with the following flux density distributions shown in Fig. 8.

B_{MODEL} curves have step shapes because they correspond to the flux density in each reluctance of the magnetic circuit and air-gap. For each curve B_{MODEL} in Fig. 8 we have 5 steps which corresponds to Rgp11, Rgp1, R6, R4 and R2 from Fig. 5. The inset in Fig. 8 presents the first two steps (zoom) up to halfway in the airgap. Going from the highest level of induction to the lowest one, each step means that some magnetic fringing flux is diverted.

In order to prove that using mean values for the geometric parameters does not change the accuracy of the model, we calculated the difference of the flux density in the air-gap between COMSOL simulations and the model by using the set of parameters in Table I (mean values) and the model without averaging the values (without mean values). We have chosen the flux density in the air-gap because it is the one that open-loop Hall-effect current sensors use for sensing. For each case, the difference versus primary current value is plotted in Fig. 9.

Clearly, there is no difference in the air-gap except for the last current value (1200 A) which is not exaggerated as an error. Thus, mean values of the geometric parameters can be used for any simulated primary current. The same conclusions have been found for the ASB magnetic core.

Now that the network topology and the geometrical parameters are identified, we can focus on the second main part

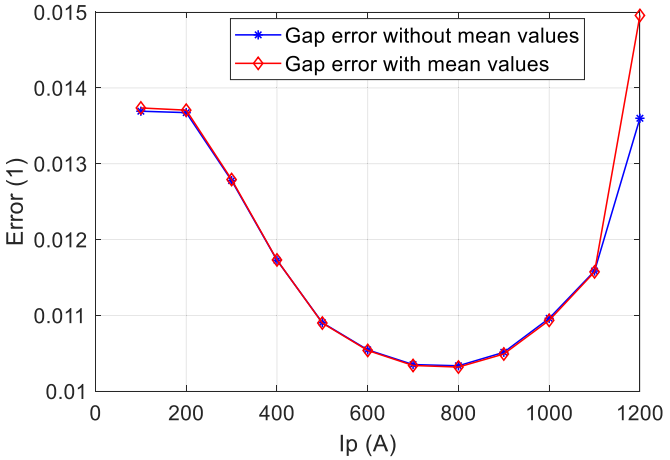

Fig. 9. Flux density error in the air-gap as a function of primary current I_P. The error is the difference between COMSOL and MODEL result in the air-gap. The curve in blue is regarding the MODEL without the use of average geometric parameters and the curve in red is regarding the MODEL with the use of average geometric parameters.

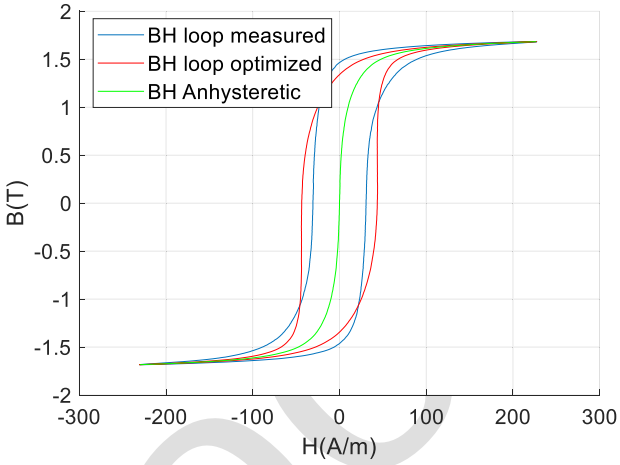

Fig. 10. BH loop measured at 100 Hz and at imposed sinusoidal flux density (1.7 T) compared to optimized one. The Anhysteretic curve corresponds to the mean curve between the ascendant and descendant parts of the measured BH loop.

of the identification which consists in building dynamic flux tubes (replacing reluctances) and specific components able to work in transient simulations.

2) Magnetic Material Modelling: The dynamic magnetic material model is based on the following equation:

$$H_{dyn}(B) = H_{stat}(B) + \gamma \times \frac{dB}{dt} \qquad (1)$$

Assumptions, limits, and rules of use of this model are fully detailed in [9]. The dynamic excitation field (H_{dyn}) is assumed as the sum of a static field (H_{stat}) that depends on the value of B (flux density) and the value of the derivative dB/dt multiplied by a dynamic parameter γ that must be identified.

In our case, $H_{stat}(B)$ is just a quasi-static anhysteretic non-linear function as shown in Fig. 10.

The value of γ is determined by comparing the simulated and measured hysteresis loops obtained on an oblong Fe-Si closed magnetic core (without air-gap) with a sinusoidal flux density waveform of amplitude B = 1.7 T at the frequency of 100 Hz. AMH-200K-S of LABORATORIO ELECTRO FISICO was used as a hysteresis measurement equipment.

After identification, the obtained dynamic parameter γ is 0.0412. Fig. 10 shows the measured and the optimized hysteresis loops.

E. Specific Components Implementation in LTspice

Three specific components were built, and symbols were created on LTspice software to model the whole sensor more easily. These components are the magnetic circuit flux tube, the air flux tube, and the winding.

1) Magnetic Circuit Flux Tube: This magnetic component concerns the flux tubes that will represent the magnetic circuit reluctances (R_1 to R_6). This component holds the dynamic model (equation (1)). The equation can be expressed in terms of magneto-motive forces and fluxes by introducing L_m (average length of the considered reluctance) and S_{cm} (cross-section of the magnetic circuit).

$$H_{dyn} \times L_m = L_m \times H_{stat}\left(\frac{\phi}{S_{cm}}\right) + L_m \times \frac{\gamma}{S_{cm}} \times \frac{d\phi}{dt} \qquad (2)$$

The latter equation is implemented with a behavioural voltage source (BV) and a resistor as shown in Fig. 11 a.

2) Air Flux Tube: With the employed analogy, a simple capacitor (which represents the permeance of an air flux tube) is sufficient to represent flux paths in the air (airgap and fringing field paths). The component is presented on Fig. 11 b.

3) Winding Component: It is a component that allows the passage from electric quantities (expressed in volts and amperes) to magnetic ones (magnetomotive forces and flux derivatives expressed in A and Wb/s respectively). This component is modelled thanks to two behavioural voltage sources and one resistor (electrical resistance of the winding) as shown in Fig. 11 c.

4) Whole Model of the Open Loop Sensor Magnetic Core: With all the components made so far, it is very easy to build the whole model of the sensor shown in Fig. 5. The built whole sensor model is presented in Fig. 11 d.

III. Results on the Whole Sensor Model

The model is validated using three types of measurements:

- The linearity measurements,
- The bandwidth measurements,
- The response time measurements (di/dt).

The linearity is validated on the ALB and ASB sensors, but the bandwidth and the time response are validated with a commercialized LEM sensor HAH3 1200 S07/SP3 [10]. All the validation experiments were made at room temperature.

A. Linearity Validation

The measurements were made using a Data Acquisition System which is an assembly of different devices (DC suppliers, Digital Multi-Meters, High precision current sensor, DC voltage suppliers, …) all managed using LabView. Sequencies

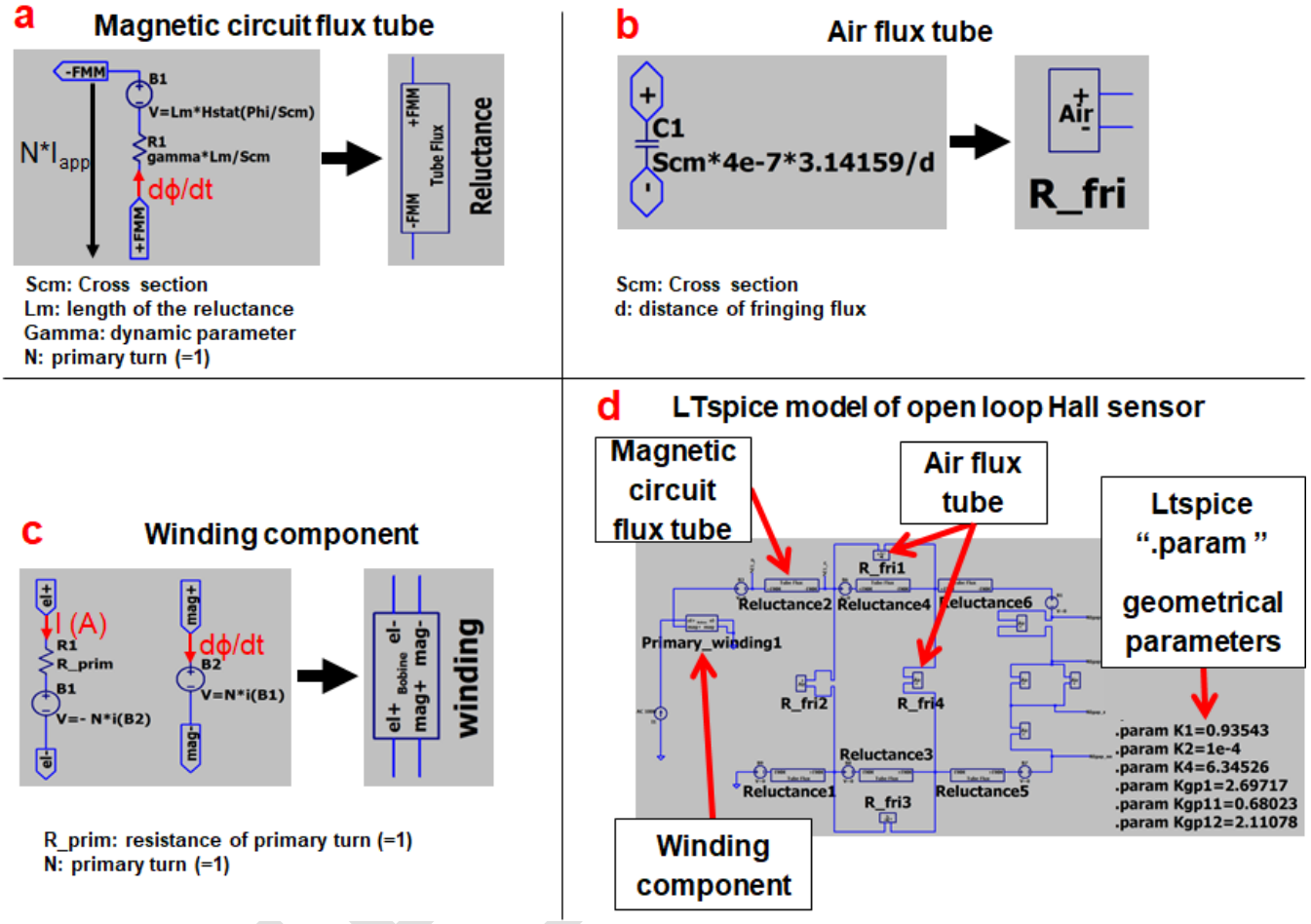

Fig. 11. LTspice magnetic components. **a**: magnetic flux tube; **b**: air flux tube; **c**: winding component. They are assembled following the proposed network topology to build the LTspice model of open loop Hall sensor presented in **d**. All the parameters (including the geometric and dynamic parameters) are introduced in their corresponding magnetic components thanks to ".param" option.

can be programmed to lunch automated measurements, for example to apply a specific current profile and/or a specific temperature profile.

The linearity measurement principle is illustrated in Fig. 12. Indeed, the current measured by the tested sensor is compared to the reference current measured by the high precision sensor. The applied current profile starts with 100 A to 1100 A with a step of 100 A.

The figures Fig. 13 and Fig. 14 show the comparison between the LTspice simulated linearity and the measured linearity for the ALB and ASB, respectively. Two linearity errors are chosen to evaluate the differences between the measurement and the simulation linearity: 0.5 % and 1 %.

Globally, the curves behave the same way. The model overestimates by 65 A at 0.5 % linearity error and by 90 A at 1 % linearity error. This means that the model can predict the current limit where the linearity errors exceed 0.5 % and 1 % with good accuracy (6 % and 7.9 % respectively) for the ALB core sensors.

The model represents the ASB sensor behaviour too. The model also overestimates by 65 A at 0.5 % linearity error and by 73 A at 1 % linearity error. This means that the model can predict the current limit where the linearity errors exceed 0.5 % and 1 % with good accuracy (7.2 % and 7.9 % respectively) for the ASB core sensors.

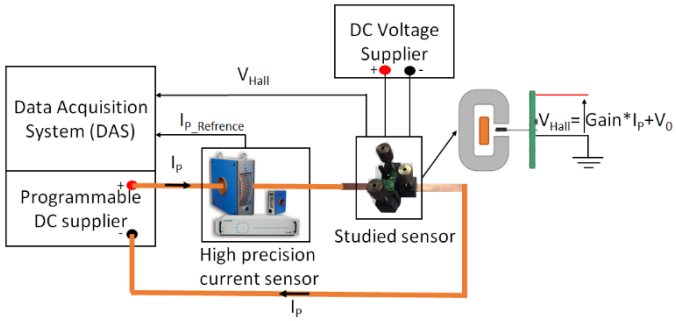

Fig. 12. Linearity test bench functioning principle. The DAS applies an increasing current profile through the DC suppliers. The applied current is measured by the high precision current sensor and by the tested sensor through its Hall die placed in the centre of the air-gap. The Hall die was calibrated accordingly to the magnetic circuit. The DAS collects the measurements for data post-processing.

B. Bandwidth Validation

The measurements were made using the experiment shown in Fig. 15. The AC supplier was set as follows:

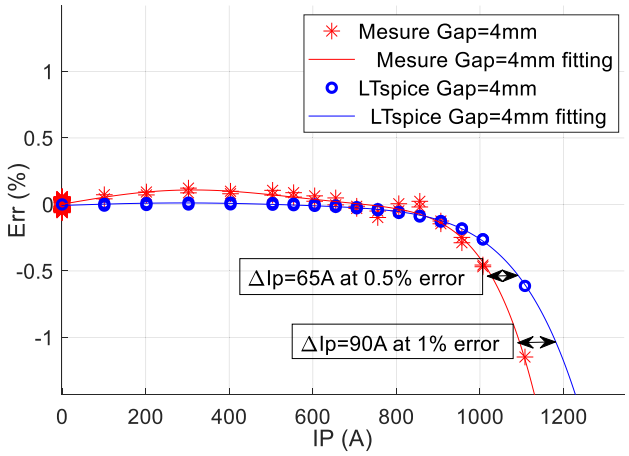

Fig. 13. Linearity for ALB core at I_{Pn} = 600 A. The magnetic circuit of an open loop Hall effect sensor is always designed according to the nominal current I_{Pn} and maximal current I_{Pmax} of a given application.

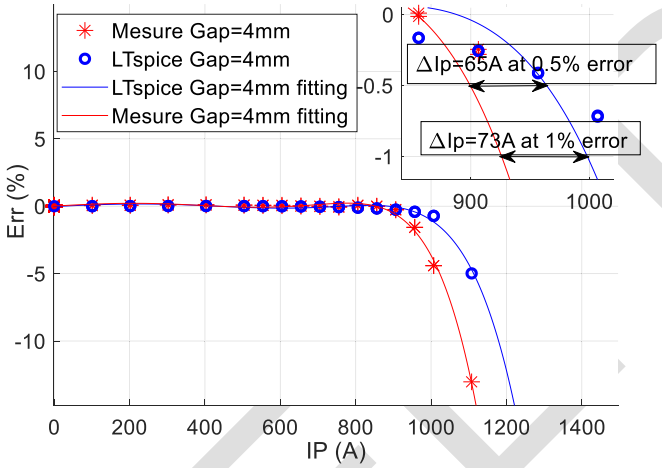

Fig. 14. Linearity for ASB core at IP_n = 600 A. The magnetic circuit of an open loop Hall effect sensor is always designed according to the nominal current I_{Pn} and maximal current I_{Pmax} of a given application.

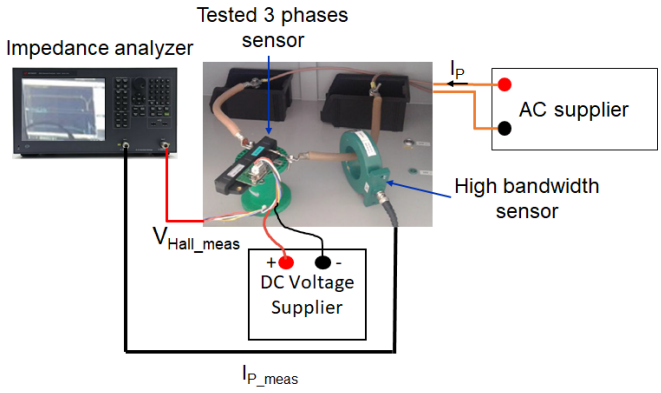

Fig. 15. Bandwidth measurement functioning principle. The DC voltage supplier is used to feed up the tested sensor.

- Peak current of 20 A,
- Sine waveform,
- Sweep frequency from 10 Hz to 100 kHz.

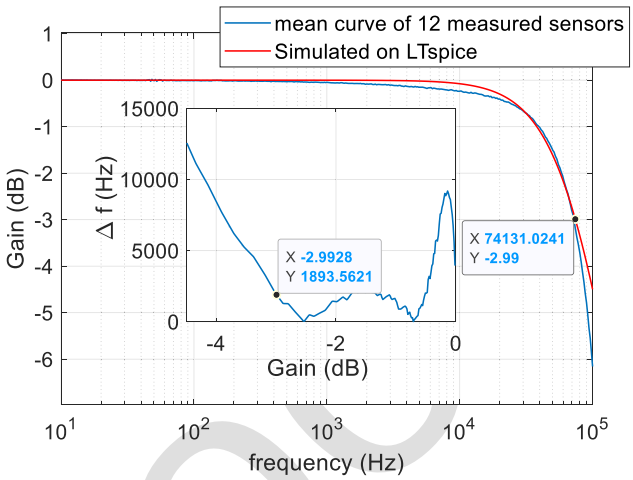

Fig. 16. Bode gain plot and frequency difference. The inset shows the frequency difference between measurement and simulation as a function of the gain.

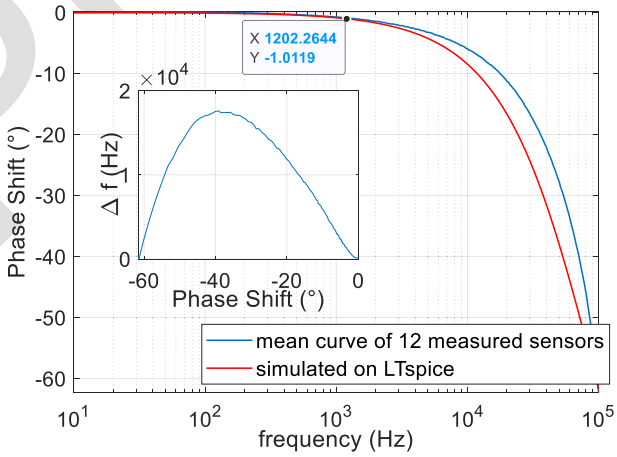

Fig. 17. Bode phase plot and frequency difference. The inset shows the frequency difference between measurement and simulation as a function of the phase shift.

The impedance analyzer calculates the gain and the phase shift by comparing the injected AC current measured with the high bandwidth sensor to the current measured with the 3 phases sensor. Five sensors were submitted to the test. Thus, in total 12 phases (monophase sensors) were measured.

The mean curves of the 12 sensors are considered as the reference. The LTspice bandwidth simulation is made in the same conditions as the measurements (except that it is done only once).

Fig. 16 and Fig. 17 show, respectively, the Bode gain plot and Bode phase plot for the simulation and the measurement. The model can provide Bode plots with good accuracy.

Quantitatively, in the case of the Bode gain plot, the model accurately fits the targeted values between −1 and −3 dB which corresponds to frequencies approximately between 20 kHz and 75 kHz. Indeed, in this interval, the frequency error is very low (Δf is less than 2.1 kHz) as shown in the inset of Fig. 16. For the Bode phase plot, the model precisely fits the targeted values of less than 1° phase shift which

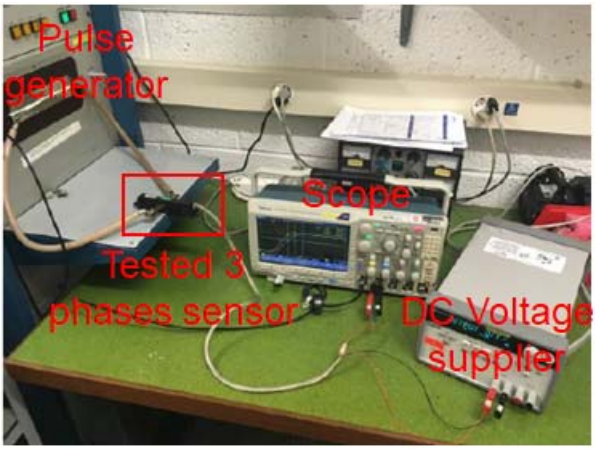

Fig. 18. Response time experiment. The DC voltage supplier is used to feed up the tested sensor.

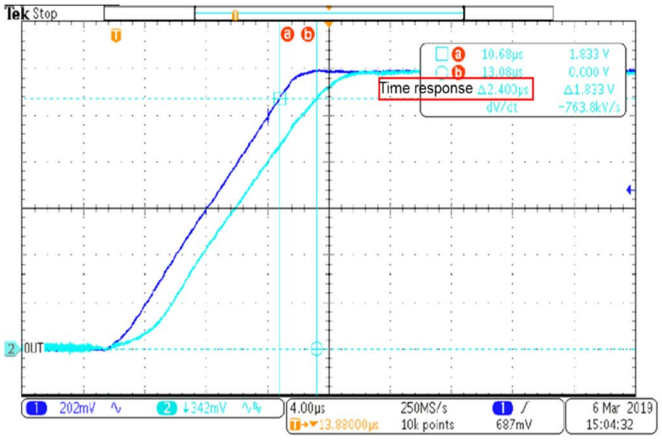

Fig. 19. Current step signal scop screenshot of the sensor 12. The red rectangle shows the time response at 90% of the primary signal.

TABLE II
SUMS UP THE RESPONSE TIMES FOR THE 12 SENSORS

Sensors	t_r (µs)
Sensor 1	1.84
Sensor 2	2.4
Sensor 3	2.28
Sensor 4	1.56
Sensor 5	1.96
Sensor 6	2.44
Sensor 7	1.72
Sensor 8	2.00
Sensor 9	2.28
Sensor 10	1.44
Sensor 11	2.2
Sensor 12	2.4

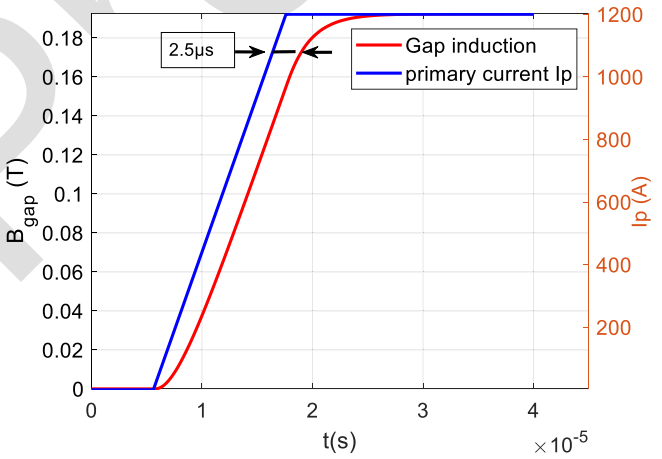

Fig. 20. Simulated di/dt step signal of the LTspice model. At 90% of 1200 A, the response time is 2.5μs.

corresponds approximately to 1.2 kHz. Indeed, the frequency error is less than 250 Hz as shown in the inset of Fig. 17. Beyond 1° phase shift, the accuracy of the model decreases (frequency difference increases). The phase is generally much more difficult to predict than the gain, so this result is not surprising.

It is to notice that the simulations did not include the Hall die frequency behaviour because its bandwidth response is very large compared to the magnetic circuit. Indeed, [11] shows that the −3 dB gain frequency is around a few hundreds of kHz and the 1° phase shift frequency is around a few tens of kHz.

C. Response Time Validation

The measurements were made using the experiment shown in Fig. 18. The pulse generator was set as follows:

- Peak current of 1200 A,
- A step signal with slope of 100 A/μs.

A Scope was used to visualize the shunt voltage which is the image of the injected pulse current, and the Hall voltage measured by the tested 3 phases sensor. The response time is calculated at 90 % of the shunt voltage that corresponds to 1200 A.

As for the bandwidth measurements, 5 three phases' sensors were submitted to the response time test. Thus, in total 12 phases (monophase sensors) were measured.

The table below summarizes the calculated response times for the 12 measured sensors.

The mean value is around 2 μs.

Fig. 19 shows an oscilloscope screenshot of a dv/dt (image of di/dt) measurement of sensor 12.

The blue curve is the shunt voltage of the primary current and the cyan curve is the Hall output voltage of the tested sensor. As shown with cursors, the sensor 12 responds with $t_r = 2.4$ μs.

The output Hall voltage is proportional to the flux density in the airgap. Neglecting the response time of the Hall probe, the response time of the LTspice model is evaluated by measuring directly the induction in the air-gap. Indeed, the Hall die

AQ:7

TABLE III
COMPARISON OF THE PROPOSED MODEL TO PREVIOUSLY PUBLISHED ONES

		Reluctance network model	Model of [6]	Model of [5]	Model of [15]	Model of [11]
Complexity		medium	medium	medium	high	low
Precision		high	medium	medium	high	Not evaluated
hysteresis model		Equation (1)	Equation (1)	Play-model [5], [16]	Preisach [17]	Core-less
Application		Open-loop Hall effect sensor	Closed-loop Hall effect sensor	Transformer	Open-loop Hall effect sensor	Core-less Hall effect sensor
Experimental validation	Linearity	medium	n/a	n/a	n/a	n/a
	Bandwidth	High at -3dB and 1°	n/a	n/a	n/a	n/a
	Time response	high	n/a	n/a	n/a	n/a
	other	n/a	High Validation made on a transformer with air-gap	High Validation made on a transformer without air-gap	High Validation made at different frequencies	n/a

TABLE IV
SIMULATION TIME CONSUMPTION

	LTspice	COMSOL
Linearity (100 A: 100: 1200 A)	1-2 seconds	2-3 minutes
Bandwidth (20 A ; 10 Hz→100 kHz)	Instantaneous	6-7 hours

response time is depending on the spinning frequency of the bias current [11]–[14] which is greater than 8 MHz.

Fig. 20 shows the LTspice model response to the $\mathrm{d}i/\mathrm{d}t$ step signal. At 90% of 1200 A, the response time is 2.5μs.

If we consider the measured response time mean value of 2 μs, the model deviates by only 0.5 μs for the worst case, which is highly precise. The response time accuracy is mainly related to the dynamic parameter γ. Thus, the identification must be done with high precision.

Table III exhibits a qualitative comparison between the proposed model and other magnetic models. Only few models were found in literature that includes the magnetic circuit behaviour.

IV. CONCLUSION

In this paper, a generic reluctance network model of the magnetic core of open-loop Hall effect current sensors with a dedicated identification protocol is presented. It is shown that the geometrical parameters to identify are independent of the current level. Thus, only one set of parameters is necessary to simulate the sensor's response for any current amplitude and waveform.

The added value of the specific components implementation in LTspice (dynamic flux tubes, air tubes and winding components) allows predicting exact results before the prototyping phase. First, the model linearity results show good agreement with the measurements for the two magnetic cores (ALB and ASB). The current limit of linearity for 0.5 % or 1 % error is predicted by the model with an accuracy below 10 % for both types of sensors. Secondly, the frequency behaviour of the sensor is also predictable by the established model. It has been found that between -0.5 dB and -3 dB, the model predicts the frequencies with an error below 2 kHz in the range of 20 kHz to 70 kHz. The phase shift diagram predicted by the model gave good results too until 1°. After that, the error between the model and the measurements diverges, as the phase shift is generally much more difficult to predict with accuracy. Finally, the response time of the sensor can also be estimated by our model with an error below 0.5 μs for the worst case. Now that the model of the oblong magnetic circuit with air gap is validated, engineers can, for any design:

- Simulate all types of current waveforms,
- Identify trends by varying the geometric dimensions (in a small range: air gap, cross-section, …),
- Estimate frequency bandwidths,
- Estimate the response time, in a very short time.

A time consumption estimation is done considering LTspice and COMSOL linearity and bandwidth simulations.

Clearly, using the LTspice model will save much time.

As the proposed model (and the associated protocol) can also be used to describe other devices under the condition that the magnetic core geometry remains close to the oblong shape and to the studied dimensions, engineers can also work on the design of electronic circuits for closed-loop Hall effect sensors. If the geometry and/or the dimensions are completely changed, the identification protocol presented in the paper can be easily reused/readapted because the protocol has been fully automated using the COMSOL "LiveLink Matlab" module. Thanks to the model developed in this paper, engineers can give some preliminary answers during the design phase, before the generally more costly prototyping phase.

REFERENCES

[1] L. Guo, C. Xia, H. Wang, Z. Wang, and T. Shi, "Improved equivalent magnetic network modeling for analyzing working points of PMs in interior permanent magnet machine," *J. Magn. Magn. Mater.*, vol. 454, pp. 39–50, May 2018, doi: 10.1016/j.jmmm.2018.01.018.

[2] D. Faustner, W. Kemmetmüller, and A. Kugi, "Magnetic equivalent circuit modeling of a saturated surface-mounted permanent magnet synchronous machine," *IFAC-PapersOnLine*, vol. 48, no. 1, pp. 360–365, 2015, doi: 10.1016/j.ifacol.2015.05.033.

[3] M. Farhadian, M. Moallem, and B. Fahimi, "Analytical calculation of magnetic field components in synchronous reluctance machine accounting for rotor flux barriers using combined conformal mapping and magnetic equivalent circuit methods," *J. Magn. Magn. Mater.*, vol. 505, Jul. 2020, Art. no. 166762, doi: 10.1016/j.jmmm.2020.166762.

[4] D. Cao, W. Zhao, J. Ji, L. Ding, and J. Zheng, "A generalized equivalent magnetic network modeling method for vehicular dual-permanent-magnet Vernier machines," *IEEE Trans. Energy Convers.*, vol. 34, no. 4, pp. 1950–1962, Dec. 2019, doi: 10.1109/TEC.2019.2921699.

[5] Y. Hane and K. Nakamura, "Hysteresis modeling of magnetic devices based on reluctance network analysis," in *Proc. Int. Power Electron. Conf. (IPEC-Niigata-ECCE Asia)*, Niigata, Japan, May 2018, pp. 2426–2429, doi: 10.23919/IPEC.2018.8507646.

[6] F. Sixdenier and M. A. Raulet, "Current sensor modeling with a FE-tuned MEC: Parameters identification protocol," *IEEE Sensors J.*, vol. 12, no. 5, pp. 859–863, May 2012, doi: 10.1109/JSEN.2011.2165841.

[7] V. Litovski and M. Zwolinski, *VLSI Circuit Simulation and Optimization*. Accessed: Feb. 23, 2022. [Online]. Available: https://link.springer.com/book/9780412638602

[8] W. J. McCalla, *Fundamentals of Computer-Aided Circuit Simulation*. Springer, 2012.

[9] M. Raulet, F. Sixdenier, B. Guinand, L. Morel, and R. Goyet, "Limits and rules of use of a dynamic flux tube model," *COMPEL Int. J. Comput. Math. Electr. Electron. Eng.*, vol. 27, no. 1, pp. 256–265, Jan. 2008, doi: 10.1108/03321640810836816.

[10] *HAH3DR 1200-S07/SP3 | LEM*. Accessed: Feb. 23, 2022. [Online]. Available: https://www.lem.com/en/hah3dr-1200s07sp3

[11] M. Crescentini, S. F. Syeda, and G. P. Gibiino, "Hall-effect current sensors: Principles of operation and implementation techniques," *IEEE Sensors J.*, early access, Oct. 13, 2021, doi: 10.1109/JSEN.2021.3119766.

[12] H. Fan, S. Li, Y. Cen, Q. Feng, and H. Heidari, "A horizontal Hall sensor 3D comsol model," in *Proc. IEEE 63rd Int. Midwest Symp. Circuits Syst. (MWSCAS)*, Aug. 2020, pp. 893–896, doi: 10.1109/MWSCAS48704.2020.9184586.

[13] H. Heidari *et al.*, "CMOS vertical Hall magnetic sensors on flexible substrate," *IEEE Sensors J.*, vol. 16, no. 24, pp. 8736–8743, Dec. 2016, doi: 10.1109/JSEN.2016.2575802.

[14] H. Heidari, E. Bonizzoni, U. Gatti, and F. Maloberti, "Analysis and modeling of four-folded vertical Hall devices in current domain," in *Proc. 10th Conf. Ph.D. Res. Microelectron. Electron. (PRIME)*, Jun. 2014, pp. 1–4, doi: 10.1109/PRIME.2014.6872733.

[15] K. Kim, K. Hong, H. Lee, H.-S. Kim, and S.-K. Hong, "Hysteresis compensation method for measurement error of Hall effect current sensor considering eddy current effect for electric vehicle at high speed," in *Proc. IEEE Appl. Power Electron. Conf. Expo. (APEC)*, Mar. 2019, pp. 2653–2658, doi: 10.1109/APEC.2019.8721936.

[16] A. Giraud, A. Bernot, Y. Lefévre, and J. F. Llibre, "Modeling quasi-static magnetic hysteresis: A new implementation of the play model based on experimental asymmetrical B(H) loops," in *Proc. XXII Int. Conf. Electr. Mach. (ICEM)*, Sep. 2016, pp. 1895–1901, doi: 10.1109/ICELMACH.2016.7732782.

[17] F. Preisach, "Über die magnetische nachwirkung," *Zeitschrift Physik*, vol. 94, nos. 5–6, pp. 277–302, May 1935, doi: 10.1007/BF01349418.

Atef Lekdim received the master's and Ph.D. degrees in electrical engineering from Claude Bernard Lyon 1 University in 2013 and 2017, respectively. He is currently working as a Research and Innovation Engineer with LEM Tech France. LEM Company is one of the leaders in electrical sensing devices. His main research interest includes magnetic modeling and magnetic material characterization for current sensor applications.

Fabien Sixdenier (Member, IEEE) received the B.S., M.S., and Ph.D. degrees in electrical engineering from Université Claude Bernard Lyon 1, France, in 2000, 2002, and 2005, respectively.

Since 2006, he has been an Associate Professor with Université Claude Bernard Lyon 1. He is currently working on characterization and modeling of soft magnetic materials. In particular, he developed several magnetic hysteresis models implemented in finite elements and circuit type (SPICE) software that can take into account temperature. He is also working on middle frequency transformers design methodology. Dr. Sixdenier was a recipient of the Best Paper Award of the Electrical Power and Energy Conference (EPEC) in 2015.

Riccardo Scorretti received the M.S. degree in informatics engineering from the University of Florence, Italy, in 1999, and the Ph.D. degree in electrical engineering from the École Centrale de Lyon, France, in 2003. Since 2005, he has been a Researcher with CNRS. He is currently working on numerical modeling applied to numerical dosimetry and magnetic materials.

Adnan Grihe received the M.Sc. degree in electrical energy from Franche Comte University, France, in 2020. He is currently working on the development of electrical certification training for engineers and technicians working in the field of hybrid and electric vehicles. He is interested in characterization and modeling of soft magnetic materials and renewable energy.